INTERFACE

rsif.royalsocietypublishing.org

Research

Cite this article: Miyashita S, Audretsch C, Nagy Z, Füchslin RM, Pfeifer R. 2015 Mechanical catalysis on the centimetre scale. *J. R. Soc. Interface* **12**: 20141271. http://dx.doi.org/10.1098/rsif.2014.1271

Received: 17 November 2014
Accepted: 6 January 2015

Subject Areas:
biomimetics, computational biology

Keywords:
magnetic catalysis, enzyme, inhibitor, conformation change, autocatalysis, reaction phase

Author for correspondence:
Shuhei Miyashita
e-mail: shuheim@csail.mit.edu

Electronic supplementary material is available at http://dx.doi.org/10.1098/rsif.2014.1271 or via http://rsif.royalsocietypublishing.org.

THE ROYAL SOCIETY PUBLISHING

Mechanical catalysis on the centimetre scale

Shuhei Miyashita[1,2], Christof Audretsch[1,3], Zoltán Nagy[4], Rudolf M. Füchslin[5,6] and Rolf Pfeifer[1,7,8]

[1]Department of Informatics, University of Zurich, Andreasstrasse 15, 8050 Zurich, Switzerland
[2]Computer Science and Artificial Intelligence Laboratory, Massachusetts Institute of Technology, 32 Vassar St., Cambridge, MA 02139, USA
[3]Department of Bioinformatics, University of Wurzburg, Biocenter, Am Hubland, 97074 Wurzburg, Germany
[4]Department of Architecture, ETH Zurich, John-von-Neumann-Weg 9, 8093 Zurich, Switzerland
[5]Institute of Applied Mathematics and Physics, Zurich University of Applied Sciences, Technikumstrasse 9, 8400 Winterthur, Switzerland
[6]European Centre For Living Technology, S. Marco 2847, 30124 Venezia, Italy
[7]Institute of Academic Initiatives, Osaka University, 1-3 Machikaneyama, Toyonaka, Osaka, 560-8531, Japan
[8]Department of Automation, Shanghai Jiao Tong University, 800 Dong Chuan Rd, Min Hang, Shanghai 200240, China

Enzymes play important roles in catalysing biochemical transaction paths, acting as logical machines through the morphology of the processes. A key challenge in elucidating the nature of these systems, and for engineering manufacturing methods inspired by biochemical reactions, is to attain a comprehensive understanding of the stereochemical ground rules of enzymatic reactions. Here, we present a model of catalysis that can be performed magnetically by centimetre-sized passive floating units. The designed system, which is equipped with permanent magnets only, passively obeys the local causalities imposed by magnetic interactions, albeit it shows a spatial behaviour and an energy profile analogous to those of biochemical enzymes. In this process, the *enzyme* units trigger physical conformation changes of the target by levelling out the magnetic potential barrier (activation potential) to a funnel type and, thus, induce cascading conformation changes of the targeted *substrate* units reacting in parallel. The *inhibitor* units, conversely, suppress such changes by increasing the potential. Because the model is purely mechanical and established on a physics basis in the absence of turbulence, each performance can be explained by the morphology of the unit, extending the definition of catalysis to systems of alternative scales.

1. Introduction

In the biochemical realm, enzymes ($\mathcal{E}$) help substrates ($\mathcal{S}$) yield products ($\mathcal{P}$) by catalysing the activation potentials of the transition paths [1]. In a typical microscopic view of catalytic reaction $\mathcal{E}$ acts on $\mathcal{S}$, configures an enzyme–substrate complex ($\mathcal{ES}$), induces a conformation change of the substrate ($\mathcal{EP}$) and carries off with the product, $\mathcal{P}$

$$\mathcal{E} + \mathcal{S} \xrightarrow{k_1} \mathcal{ES} \overset{k_2}{\rightleftharpoons} \mathcal{EP} \xrightarrow{k_3} \mathcal{E} + \mathcal{P}. \tag{1.1}$$

Albeit an individual molecule involves complex kinematics and is difficult to engineer, each transaction phase can be regarded as a logical operation [2], and the macroscopic view of the temporal dynamics can be characterized by the corresponding reaction speeds (k_1, k_2 and k_3). While there is a discrepancy between the microscopic (mechanics) and the macroscopic (chemistry) perspectives, it has been generally considered that the key to this remarkable achievement lies in the addressability of individual molecules in representing discrete states, hidden in the morphology that rules the individual reaction order in a bottom-up manner.

Lately, a process (inspired by chemistry) in which components spontaneously organize into complex structures, (self-assembly), has gathered

attention [3]. A typical operation is, as described in chemical engineering studies, to control a global state of a system consisting of many components by regulating an environmental agitation, inducing a composition as a product. Such a synthetic process provides a new perspective for understanding biochemical reactions, and a promising path towards new manufacturing methods for complex non-molecular composition engineering (e.g. self-assembling electronic circuits) [4]. To date, various attempts at creating artificial self-assembly systems have performed simple aggregation-based assemblies, characterized by the direct *forward reaction*. The major attempts explored in the field can be represented by a reaction equation in which the components $\mathcal{S}_1$ and $\mathcal{S}_2$ are configured into $\mathcal{S}_1\mathcal{S}_2$, i.e. $\mathcal{S}_1 + \mathcal{S}_2 \rightarrow \mathcal{S}_1\mathcal{S}_2$. The components form a lattice structure after interacting mechanically [5], magnetically [6–10], electrostatically [11,12], via capillary forces [13–16], hydrophobic/hydrophilic forces [17,18], fluid dynamics [19] or through configuring circuitry [20–23]. Hereafter, we use the term *reaction* in a broad sense, including those obtained mechanically.

In contrast to the capability of assembly, disassembly or the so-called *backward reaction*, $(\mathcal{S}_1\mathcal{S}_2 \rightarrow \mathcal{S}_1 + \mathcal{S}_2)$, has attracted less attention, although it is critical for reconfiguration processes, catalytic reactions or regrouping components. These processes regularly combine with external forces to realize disassembly [24], or change the surrounding medium to alter the interaction between the components [25,26]. A unique approach focusing on the asymmetry of a membrane and its influence on the diffusion speeds of molecules is found in [27].

The engineering challenge here is to orchestrate an ordered assembly/disassembly down to individual components to globally attain a high yield of products, where the component has limited capabilities, as the available physical forces such as the electric, chemical or magnetic interactions provide limited interaction channels for the involved parts. Thus, for example, magnetism and capillary forces support only binary binding (either attraction or repulsion). A few notable attempts exist in which the emphases are placed on the logical responses of the components with respect to their possibilities of combining with the neighbour components, performing template replications [28–31], efficient crystallization [32] or exclusive-or (XOR) calculations [33]. These approaches actively exploit physical 'states' of the components (e.g. $\mathcal{S}$ versus $\mathcal{P}$), whereby the two states are realized by changes in the mechanical and/or magnetic configuration of the involved components. A state change (implicitly or explicitly) alters the terrain of the system's potential energy and, thus, has the effect of accelerating the transition from one state to another. However, little reasoning has been conducted to quantify the cause of a transition, and proposed explanations have instead been based on phenomenological descriptions with heuristically designed components. One of the reasons for this could be that the presence of environmental agitation in the system complicates these analyses (in other words, these systems are essentially open to the environment). Then, the amount of kinetic energy delivered from the environment to a component contributing to a transition over time is difficult to assess, and, thus, the component's mechanical role is difficult to evaluate in a continuous parametric space. Beyond these approaches, we expect one component to function like an enzyme, that is, to act as a third agent and enable a state switch of a targeted component $(\mathcal{S} \rightarrow \mathcal{P})$ using magnetic potential energy only, where almost no environmental agitation is applied (thus, the system is essentially closed).

Here, by demonstrating that a simple enzymatic process, described by equation (1.1), can be obtained mechanically by passive magnetic units on the centimetre-scale, we focus on deriving the mechanical design principle of this chemical reaction and show that the concept of catalysis from chemistry can be generalized to alternative fields such as engineering. The proposed model, which consists of water-floating units equipped with permanent magnets, exhibits behaviours analogous to biological enzymes, and a comparable method of energy employment that levels out the potential barrier.

2. Design principle of magnetic catalysis

This section provides a theoretical reasoning on how the magnet motion must be coordinated in space in order to attain catalytic behaviour. We assume a physical set-up where magnets with a cylindrical shape slide on a horizontal plane, guided by physical walls.

2.1. Magnetism

To realize catalytic behaviour with magnets, the trajectories of the magnets must be designed at each reaction phase, which requires knowledge of the relationships between different intermagnet distances. The magnetic potential energy between two magnets M_1 and M_j (treated as dipoles) with magnetic moments $\boldsymbol{m}_i$ and $\boldsymbol{m}_j$ $(\in \mathbb{R}^3,\ i \neq j \in \mathbb{N})$ separated by a position vector r_{ij} $(\in \mathbb{R}^3)$ connecting their centres, is given by

$$U_{ij} = \frac{\mu_0}{4\pi r_{ij}^3}\left[\boldsymbol{m}_i \cdot \boldsymbol{m}_j - 3\frac{(\boldsymbol{m}_i \cdot \boldsymbol{r}_{ij})(\boldsymbol{m}_j \cdot \boldsymbol{r}_{ij})}{r_{ij}^2}\right], \tag{2.1}$$

where $\mu_0 = 4\pi \times 10^{-7}\,\mathrm{H\,m^{-1}}$ is the permeability of free space, and $r_{ij} = ||\boldsymbol{r}_{ij}|| \gg$ the magnet diameters.

When the magnets have an axially magnetized cylindrical shape, placed vertically on a frictionless two-dimensional plane in either parallel or anti-parallel configurations (the magnet directions are denoted by *N* or *S* in the following figures), they interact laterally. Assuming that the magnets feature the same magnetic moment magnitude $||\boldsymbol{m}_i|| = ||\boldsymbol{m}_j|| = m$, the potential and resulting forces are simplified to

$$U_{ij} = -\sigma_{ij}\frac{\mu_0}{4\pi}\frac{m^2}{r_{ij}^3} \tag{2.2}$$

and

$$F_{ij} = -\frac{\mathrm{d}U_{ij}}{\mathrm{d}r} = -\sigma_{ij}\frac{3\mu_0}{4\pi}\frac{m^2}{r_{ij}^4}, \tag{2.3}$$

where $\sigma_{ij} = 1$ if the magnets are anti-parallel, i.e. the two magnets are attracted along the line that connects them, and $\sigma_{ij} = -1$ if they are parallel, i.e. repelling. We can determine the potential energy of the system, considering all involved magnets, from

$$U_{\mathrm{total}} := \sum_{i<j} U_{ij}. \tag{2.4}$$

If the magnets are free to move, they will move such that the total energy is reduced $(\mathrm{d}U_{\mathrm{total}}/\mathrm{d}r < 0)$, and, consequently, their relative distance is reduced (for an attractive configuration). This behaviour is the basis for designing the motion of the magnets in this work.

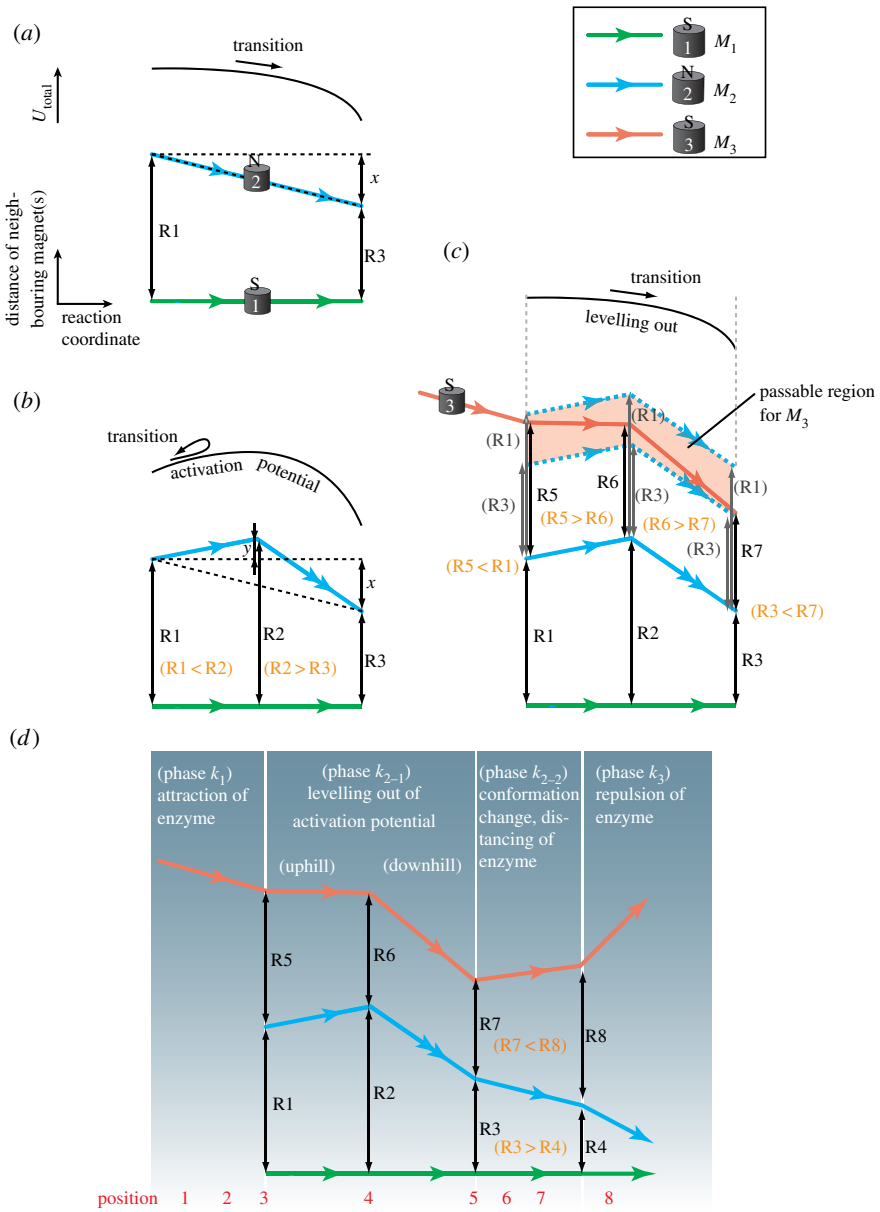

Figure 1. Incremental design of the enzymatic process. The lateral paths that M_1, M_2 and M_3 follow are shown with green, blue and red lines, respectively. (*a*) Sliding motion of magnets which can potentially perform work; i.e. change the physical conformation of the units. (*b*) Activation potential. The energy profile of the outwardly wedged paths hinders the sliding motion of the magnets. The necessary conditions on the path distances are shown in orange parentheses. (*c*) Proposed magnetic catalysis. A third magnet M_3 levels out the activation potential, acting as an enzyme, escorting M_2 to overcome the potential barrier. The distances displayed are labelled in parentheses. The passable region for M_3 derived from equation (2.5) is shown in pink. Dotted lines designate the boundaries of the path region and cannot be paths themselves. (*d*) Extension of (*c*) representing the complete enzymatic action, consisting of five distinctive phases. The position numbers 1–8, coloured in red, represent reaction stages and correspond to the same numbers in figure 2. (Online version in colour.)

Equations (2.1)–(2.4) hold strictly for $r_{ij} \gg$ the magnet diameters, and they gradually lose accuracy as r_{ij} becomes comparable to the diameters. However, because our model mostly needs to take the relative distances of magnets sets into account, they satisfy our requirements; in equation (2.3), the magnitudes of magnetic force strength are related to the relative distances, cancelling out the inaccuracy of their values.

The proposed magnetic catalysis is phenomenologically described in figure 1*a–d*, which provides the incremental design of the paths for the three magnets involved in the enzymatic behaviour. The horizontal dimension is the reaction coordinate, and the vertical dimension is the distance between neighbouring magnets. Note that all the magnets maintain the same horizontal coordinate positions. The paths are illustrated as straight lines for intuitive apprehension, even though the reaction speed along the horizontal axis is non-linear. This maintains the generality of the path descriptions, because a curved function can be approximated by a combination of linear lines. We illustrate the profile of the system's potential energy U_{total} on top of each transition path. The state of the system is characterized by the motions of the involved magnets.

2.2. Sliding motion and conformation change

In figure 1*a*, if the paths of magnets M_1 and M_2 (anti-parallel) converge by a distance x (R1 > R3; $x := \mathrm{R1} - \mathrm{R3} > 0$), the magnets slide owing to the increasing magnetic attraction force, which, in turn, reduces the relative distance (R2 is not

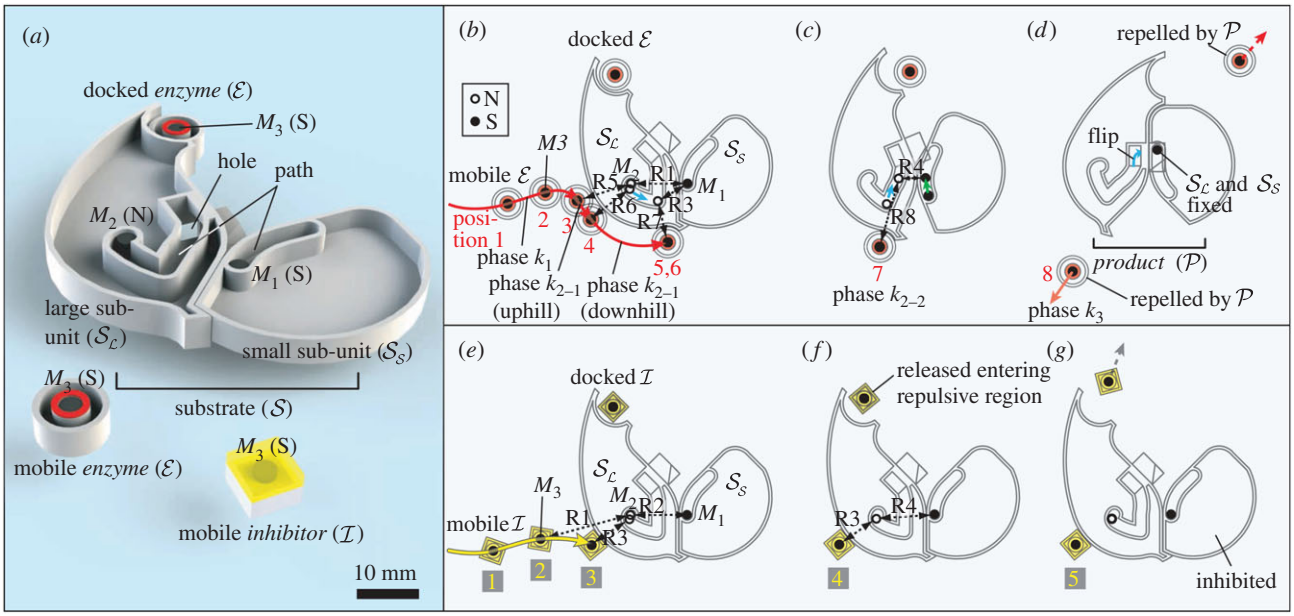

Figure 2. Physical model for the proposed enzymatic action, substantiated from figure 1*d*. (*a*) Overview of the designed floating units. (*b–d*) Magnetic catalysis by an $\mathcal{E}$ invoking a conformation change of $\mathcal{S}$, forming a different configuration $\mathcal{P}$; *product*. The paths of the magnets are shown in the same colours as in figure 1, with the corresponding labels R1–R8. (*e–g*) Inhibition of the conformation change by an $\mathcal{I}$. (Online version in colour.)

listed). The energy release can be used to perform work, which enables a kinematic reconfiguration.

2.3. Activation potential

The rate of physical convergence of the paths is a regulative parameter in the design. This is shown in figure 1*b*, where the choice of R1 < R2 ($y := \mathrm{R2} - \mathrm{R1} > 0$) and hence R2 > R3 create an outward wedged path acting as a 'threshold', which can suppress the sliding motion. Consequently, the magnets must overcome a potential energy barrier—which can be interpreted as the magnetically created activation potential—before the reaction can proceed.

2.4. Catalysis

Figure 1*c* illustrates the designed magnetic catalysis. The paths for M_1 and M_2 are the same as in the two-magnet case discussed in figure 1*b*, whereas the introduction of M_3 helps the trapped magnet M_2 to overcome the potential barrier and advance further on the path. When M_3 is attracted towards M_2, it can reach a position where the distance to M_2 (R5) becomes shorter than the distance between M_1 and M_2 (R1). Once R1 > R5 is satisfied, and the M_3–M_2 attraction exceeds that of M_1–M_2, M_2 begins its translation escorted by M_3. Note that, owing to the quick spatial decay of the magnetic force, the net force on M_2 is always dominated by the closest distance to any another magnet, and we neglect the magnetic crosstalk of the non-neighbouring magnets M_1 and M_3. By designing the distances in the paths as R5 > R6 and R6 > R7, we can ensure that M_2 reaches an endpoint where the distance from M_2 to M_1 is again closer than to M_3 (R3 < R7). In the end, incorporating all the distance relations above, we obtain the condition for designing paths for catalysis

$$\mathrm{R3} < \mathrm{R7} < \mathrm{R6} < \mathrm{R5} < \mathrm{R1} < \mathrm{R2}, \tag{2.5}$$

which draws the magnitude relations anticlockwise in the figure, starting from R3. Given R1, R2 and R3, we show the passable region for M_3 in pink, which certifies that as long as M_3 transits in this region, the reaction will proceed. The opposite happens in figure 1*b*, where the reaction stops. In this case, the system proceeds with the reaction implying that the terrain of U_{total} is levelled out (see the mathematical proof in appendix B). Note that the condition derived in equation (2.5) holds even if the interaction force depends on a different power of the distance, when $F_{i,j} \propto r_{i,j}^{-X}$ ($X \in \mathbb{N}$).

2.5. Enzymatic reaction

Figure 1*d* shows the complete enzymatic reaction, which is composed of five distinctive phases. Each magnetic reaction phase can be viewed in correspondence to the three reaction phases, k_1, k_2 and k_3, in equation (1.1). Phase k_1 is when M_3 is far away, approaching M_2. Phase k_2 is further divided into two subphases, where phase k_{2-1} represents the event when the activation potential is levelled out, and phase k_{2-2} represents the event when the energy is used for work, i.e. conformation change and distancing M_3. From a mechanical standpoint, phase k_{2-1} can be divided into two subphases, which correspond to the two sectors of the original activation potential, i.e. the uphill and downhill sectors, respectively. Phase k_{2-2} is similar to phase k_{2-1}, in that all three magnets are moving, except the driving force is now between M_1 and M_2. M_1 and M_2 attract each other, decreasing the relative distance and performing the conformation change (R3 > R4). Eventually, the distance between M_2 and M_3 is sufficiently large to reduce the net magnetic force on M_3 considerably (R7 < R8). Phase k_3 is the stage when M_3 is magnetically repelled. In our case, we designed the physical path of M_2 such that M_2 flips and changes polarity (see details in §3).

3. Physical substantiation

3.1. Units

Figure 2*a* shows an image of the designed units that implement the three paths described in figure 1*d*. The red

path represents the movement of M_3 embedded in a circular unit $\mathcal{E}$ called *enzyme*. Two paths, the green path for M_1 and blue for M_2 are mechanically arranged and embedded in the small $\mathcal{S}_S$ and the large $\mathcal{S}_L$ subunit as guiding walls for the magnets. Together, $\mathcal{S}_S$ and $\mathcal{S}_L$ compose the *substrate* $\mathcal{S}$. As the motion of the conformation change can be arbitrary, it is implemented such that $\mathcal{S}_L$ and $\mathcal{S}_S$, which rotate through a relative angle 90°, switch contact facets and in so doing mechanically simulate a protein's folding motion, forming a different configuration ($\mathcal{P}$; *product*). In addition, expecting to realize autocatalytic behaviour, we placed another $\mathcal{E}$ encapsulated in $\mathcal{S}_L$ (this second $\mathcal{E}$ is called the docked $\mathcal{E}$ in contrast to the mobile $\mathcal{E}$). The docked $\mathcal{E}$ is positioned far from M_2, and, hence, has a small effect on the interactions of the other magnets; the existence of the docked $\mathcal{E}$ is not necessary for $\mathcal{S}_S$ and $\mathcal{S}_L$ to maintain the configuration of $\mathcal{S}$.

3.2. Enzymatic reaction

The behaviour of an enzymatic reaction is illustrated in figure 2*b–d*, where the phases k_1–k_3 comprise distinguishable stages represented by the positions of the mobile $\mathcal{E}$ (tagged with positions red-1 to red-8). In brief, a mobile $\mathcal{E}$ approaching from the left triggers a conformation change of $\mathcal{S}$, releasing the docked $\mathcal{E}$, whereas it itself eventually moves away from $\mathcal{S}$ after a short contact. More concretely, the mobile $\mathcal{E}$ sits on the long-arc edge of $\mathcal{S}_L$, further rolls along it to a certain position where the distance between M_2 and M_3 (R5) becomes shorter than between M_1 and M_2 (R1; phase k_1, positions red-1 to red-3). Note that the magnets, just as well as $\mathcal{E}$, can reduce the friction with the side walls by rolling. Then, $\mathcal{E}$ drags M_2, by continuing to roll along the edge of $\mathcal{S}_L$ (phase k_{2-1} uphill and downhill, positions red-3 to red-5), until the distance between M_1 and M_2 becomes shorter than that between M_2 and M_3 (R3 < R7). Then, the attraction between M_2 and M_1 initiates a conformation change by sliding along their respective paths, decreasing the relative distance (phase k_{2-2}, positions red-6 to red-7). Eventually, M_2 falls into a hole and connects to the bottom of M_1 by flipping upside-down, in the process binding the floors of $\mathcal{S}_L$ and $\mathcal{S}_S$. These longitudinally coupled M_1 and M_2 repel the mobile $\mathcal{E}$ as well as the docked $\mathcal{E}$ from $\mathcal{S}$ (phase k_3, position red-8). When the docked $\mathcal{E}$ is expelled, it can subsequently act as a new mobile $\mathcal{E}$. Hence, the number of mobile $\mathcal{E}$ is doubled after a conformation change, inducing a cascade reaction when multiple $\mathcal{S}_S$ exist. The geometry R1–R8 is reflected by the paths in figure 1*d*, drawn in a proportional scale for this substantiation.

3.3. Inhibition

Inhibition or at least the partial suppression of a chemical reaction is also a basic biochemical function primitive, realized by highly specific molecules forming complexes with other molecules. Such molecules, called inhibitors, often dock to the binding sites of enzymes via non-covalent bonding, or prohibit conformational changes of such molecules via steric hindrance. Inspired by this fact, the inhibition of the conformation change of a *substrate* is realized by making the shape of the mobile unit rectangular, but keeping the same magnetic arrangement as for $\mathcal{E}$ (this new unit is called an *inhibitor*, $\mathcal{I}$, whose role is described in figure 2*e–g*). In contrast to the case of $\mathcal{E}$, the system with $\mathcal{I}$ inhibits a conformation change by hindering the rotational motion of $\mathcal{I}$. Owing to the angular shape, the mobile $\mathcal{I}$ cannot roll along the edge of $\mathcal{S}_L$ or it requires separation of two attracting magnets M_2– M_3 (thus, the barrier would indeed be regarded as an activation potential by $\mathcal{I}$), and restricts the conformation change by trapping M_2 midway in its path (position yellow-4 in figure 2*f*). The docked $\mathcal{I}$ is nevertheless released because it is now in a repulsive region, and the number of mobile $\mathcal{I}$ is preserved to continue reactions (see the change in the attractive region in the electronic supplementary material, figure S4). Thus, $\mathcal{S}$ is magnetically inactivated; it cannot change its conformation nor attract another mobile $\mathcal{E}$ or $\mathcal{I}$. Note that reactions can proceed in parallel, because $\mathcal{E}$ and $\mathcal{I}$ act on $\mathcal{S}$, and vice versa, whereas $\mathcal{E}$s and $\mathcal{I}$s repel each other, as do the $\mathcal{S}$s.

3.4. Experimental set-up

All the units, ranging from 7.07 to 55.66 mm in diameter (see the electronic supplementary material, figure S3 for detailed dimensions), were designed using a computer-aided design program (SolidWorks) and then printed with a three-dimensional printer (Dimension BST 768) on acrylonitrile butadiene styrene[1]. The employed magnets, M_1, M_2 and M_3, have a cylindrical shape (Ø 3.0 × H 3.0 mm), weigh 0.161 g and are made of nickel-coated neodymium iron boron with a magnetic flux density of 0.340 T at the middle of the surface (supermagnete, S-03-03-N). Experiments with multiple units combined in §4.2 were conducted in a water container of Ø400 mm with 10 mm depth of water. Iron discs (Ø30.0 × H 3.0 mm) were placed below each $\mathcal{S}$ to position and maintain the initial two-dimensional coordinates of the $\mathcal{S}$s. The experiments with a single conformation change were recorded by a high-speed camera, and the magnet positions were tracked using a software (Tracker).

4. Results

4.1. Conformation change and inhibition

Figure 3 shows snapshots of a conformation change invoked by a mobile $\mathcal{E}$ (figure 3*a*), and inhibition by a mobile $\mathcal{I}$ (figure 3*b*). Figure 3*a*: a mobile $\mathcal{E}$ is attracted to $\mathcal{S}$ (−0.390 to −0.133 s; we set $t = 0$ s when the mobile $\mathcal{E}$ is in a contact with $\mathcal{S}_L$), it brings M_2 on $\mathcal{S}_L$ to the sharp bend in the path (0.095–0.186 s), induces a conformation change (0.333–0.619 s), and finally bears off from $\mathcal{S}_L$ (0.910–1.110 s). The average duration of a conformation change (over 20 trials) was 0.459 ± 0.105 s (s.d.), similar to that of the contact of $\mathcal{E}$ to $\mathcal{S}_L$ 0.456 ± 0.103 s (s.d.). In most cases, at phase k_{2-1}, M_2 moved faster than $\mathcal{E}$, giving a brief indication of the inertia of $\mathcal{E}$.

Figure 3*b*: just as for the mobile $\mathcal{E}$ in figure 3*a*, a mobile $\mathcal{I}$, which has the same magnet arrangement, is attracted to $\mathcal{S}$ (−0.619 and −0.071 s). When $\mathcal{I}$ makes contact with $\mathcal{S}_L$, it attracts M_2, but because $\mathcal{I}$ itself cannot roll along the edge of $\mathcal{S}_L$, it holds M_2 at the midpoint of its path, suppressing a conformation change (1.483 s). When this entrapment occurred, the docked $\mathcal{I}$ entered a repulsive region created by M_1, M_2 and the mobile $\mathcal{I}$, and, thus, was released from $\mathcal{S}_L$ (2.152 s). This way, the released $\mathcal{I}$ can continue the inhibition process.

Figure 3*c* displays the transitions of the system's magnetic potential energy U_{total}, derived by analysing the spatial positions of the involved magnets (for experimental plots with $\mathcal{E}$ and $\mathcal{I}$), and by the design in figure 1*c* supposing that M_1– M_3 transit coherently (for a theoretical plot without $\mathcal{E}$). We

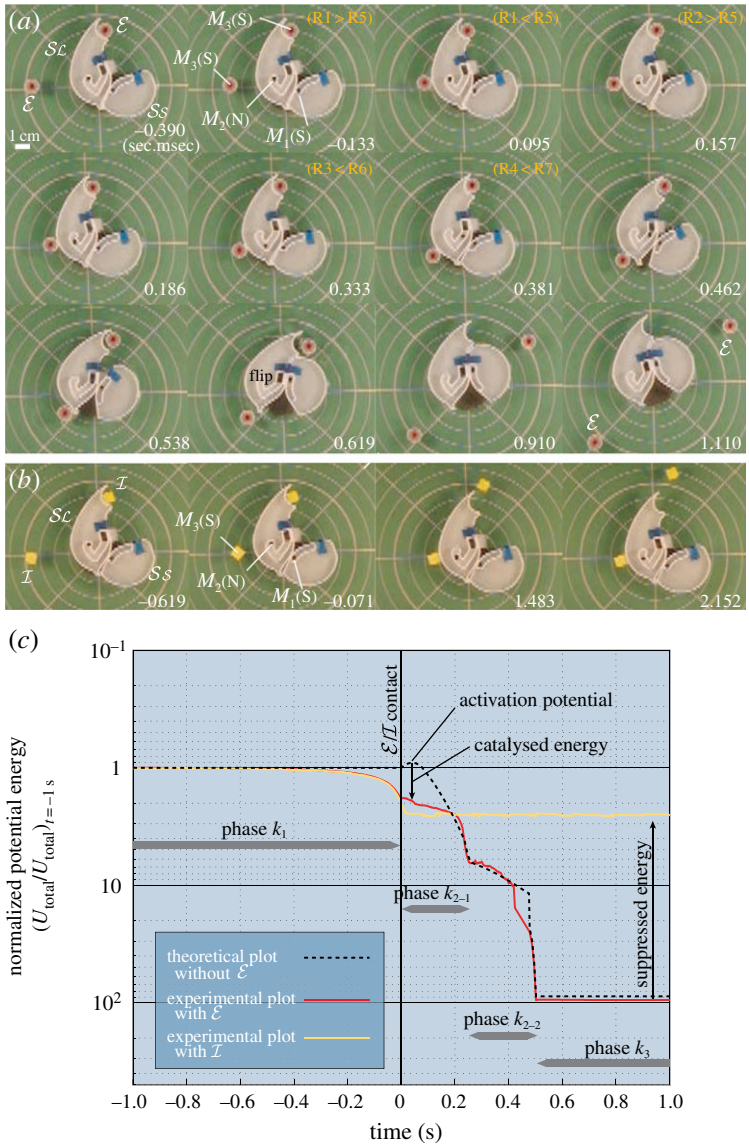

Figure 3. Snapshots of the conformation change by $\mathcal{E}$ in (*a*), inhibition by $\mathcal{I}$ in (*b*), and the derived magnetic potential energy transitions in (*c*). (*a*) A mobile $\mathcal{E}$, which is manually released at 8 cm to the left of the centre of the $\mathcal{S}$, invokes a conformation change, and moves away from $\mathcal{S}$ at the same time at which the docked $\mathcal{E}$ is released. (*b*) Owing to its angular shape, the mobile $\mathcal{I}$ cannot roll along the long edge of $\mathcal{S}_\mathcal{L}$. Hence, it remains at the same position, suppressing the conformation change by trapping M_2 at the midpoint of its path. See the electronic supplementary material (movies S1 and S2) for these two motions. (*c*) Transitions of U_{total} of (*a*), (*b*), and a theoretically derived plot assuming that the conformation change occurs without $\mathcal{E}$, all being normalized to $U_{total}|_{t=-1}$. The vertical axis is displayed in inverted form compared with figure 1 for intuitive apprehension; the lower the point on the vertical axis the lower the energy. (Online version in colour.)

normalized U_{total} by dividing by the respective U_{total} at $t = -1$ s (-1 s was determined arbitrarily, noticing the small magnetic influence of $\mathcal{E}$ and $\mathcal{I}$). In this way, the difference in the number of magnets is cancelled out. We show the vertical axis in inverted form for an intuitive understanding corresponding to figure 1.

Owing to the catalytic effect, the potential energy of $\mathcal{E}$ monotonically decreases, allowing the system to naturally proceed with reactions without an external energy input, and to reach a global stable state. By comparing the cases with $\mathcal{E}$ and the theoretically derived case without $\mathcal{E}$, the reduction in the activation energy is clearly seen (we regard this decrease as the catalysis attained by $\mathcal{E}$). Inhibition is also clearly shown in the global stable states (e.g. $t = 1$ s), because $\mathcal{I}$ suppresses the decrease in the potential energy that $\mathcal{E}$ generates. The magnitude of the energy drop by $\mathcal{I}$ is a mere 6% of that obtained with $\mathcal{E}$. As discussed, the previously defined reaction phases can be recognized as distinctive transitions.

4.2. Autocatalysis with multiple units combination

To test the designed system under more general conditions in a longer run, where multiple unit sets exist in space, we conducted experiments with five $\mathcal{E}$–$\mathcal{S}$ sets and $\mathcal{I}$–$\mathcal{S}$ sets, and show the representative trial results in figure 4. To prevent multiple $\mathcal{S}$ from gathering around the border of the container owing to their weak repulsion, we submerged iron plates 17 mm below the water surface level to weakly situate each $\mathcal{S}$, while allowing them to orient themselves in random directions. Figure 4*a* shows a trial where $\mathcal{S}$s dock $\mathcal{E}$s, whereas figure 4*b* shows $\mathcal{S}$s docking $\mathcal{I}$s. In both cases, we initiated the reactions by manually placing five $\mathcal{E}$s between the $\mathcal{S}$s, thus setting both initial conditions the same.

In figure 4*a*, after a brief interval of a quasi-stable state, the first conformation change (highlighted with a red circle) was triggered at 58.5 s, instantly followed by another conformation change at 60.1 s. The two new mobile $\mathcal{E}$s released by the conformation changes traversed the field in the 12 o'clock direction

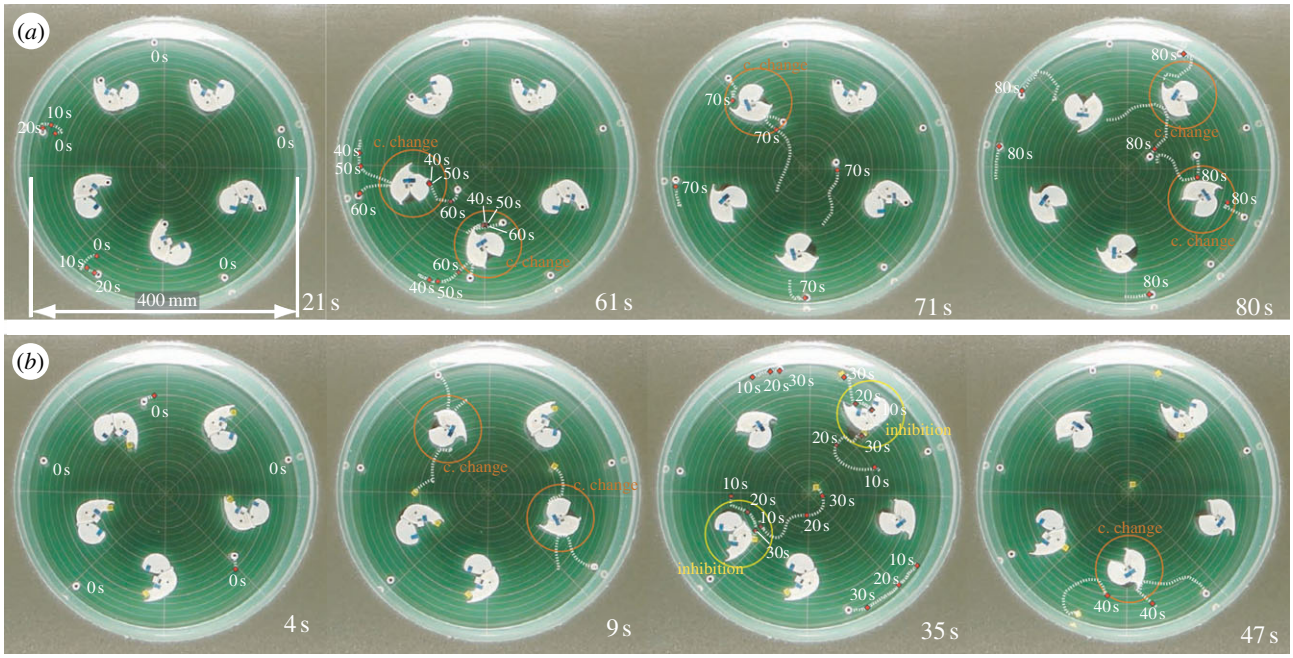

Figure 4. Snapshots of representative trials with a multiple unit combination for $\mathcal{E}$s (*a*) and $\mathcal{I}$s (*b*) pre-docked to the $\mathcal{S}$s. Each window displays the elapsed time after the placement of five $\mathcal{E}$ units, with trajectories of actively transitioning $\mathcal{E}$s and $\mathcal{I}$s. (*a*) Two of five released mobile $\mathcal{E}$s triggered conformation changes of $\mathcal{S}$s, which resulted in the remaining three triggers by the recently released $\mathcal{E}$. (*b*) Two mobile $\mathcal{E}$ that were released by conformation changes inhibited $\mathcal{S}$. See the electronic supplementary material (movies S3 and S4) for these two cases. (Online version in colour.)

following the local magnetic field gradient, and invoked two of the remaining conformation changes (70.3 and 76.6 s). The last $\mathcal{S}$ was hit by an $\mathcal{E}$ at 79.2 s, and changed its conformation. The system proceeded naturally and completed the process despite 17 of 20 magnets being involved in the series of reactions, and thus created locally complex magnetic fields. If we plot the system's energy transition as in figure 3*c*, the terrain includes sharp and significant energy drops each time a conformation change occurs. It also displays a flat terrain the majority of the time while the mobile units are travelling. The timing of the conformation changes might be affected by the density of units, though this investigation is a future research avenue.

In figure 4*b* (docked $\mathcal{I}$s), the first conformation change was triggered at 4.9 s, faster than in figure 4*a* (docked $\mathcal{E}$s). In general, the time of the first reaction is influenced by the randomly oriented $\mathcal{S}$, which, nonetheless, have little influence on the later reaction speed once a reaction starts. After another conformation change was triggered by an $\mathcal{E}$ (5.9 s), the two released $\mathcal{I}$ in the centre of the field inhibited different $\mathcal{S}$s (at 9.2 and 19.6 s, highlighted with yellow circles). The final conformation change was invoked at 40.5 s. The most significant difference from the case in figure 4*a*, the docked $\mathcal{E}$ trial, is that an inhibited $\mathcal{S}$ did not create as strong a repulsive magnetic field as in the case of $\mathcal{P}$, and hence it had less influence on the motion of the mobile units close by.

We conducted 30 trials for each of the two cases. The average durations for completing five reactions were 67.7 s (min = 13.3, median = 55.7, max = 146.3) with docked $\mathcal{E}$, and 58.6 s (min = 11.5, median = 55.3, max = 142.7) with docked $\mathcal{I}$. During the docked $\mathcal{I}$ trials, there were 36 inhibitions within 150 reactions, which corresponds to 24.0% of the total number of reactions. By considering the number of invoked conformation changes, the average duration per conformation change was 13.5 s (min = 2.7, median = 11.2, max = 29.3) and 15.9 s (min = 13.3, median = 55.7, max = 146.3) with docked $\mathcal{E}$ trials and docked $\mathcal{I}$ trials, respectively. The small difference in the durations is mainly because we began with 5$\mathcal{E}$s in both cases and, hence, the influence of $\mathcal{I}$s was screened.

During the experiments, a small number of trials were considered to be accidental errors, for example, because of magnets that jumped from $\mathcal{S}$ when changing conformation (this occurred five times before we reached 30 trials with $\mathcal{E}$s), and that failed to conduct magnet flips (this occurred five times under the same conditions with $\mathcal{E}$s). We also once terminated a trial with $\mathcal{E}$s when no reaction occurred for more than 1 minute. Considering that conformation changes with a single $\mathcal{S}$ were reliable, the increase in the failure rate seems to indicate the magnetic influence of distant magnets. Within 41 potential inhibitions, $\mathcal{I}$ did not hold its position but slipped along the edge of $\mathcal{S}_\mathcal{L}$ and invoked a conformation change on five occasions (failure rate 12.2%).

5. Discussion

Unlike highly stochastic molecular reactions where thermal agitation is the driving force for transportation and massive rapid samplings of configurations for conformation change, our system rather exhibits a deterministic behaviour, whose dynamics could thoroughly be predicted by considering the positions of all involved magnets. Our emphasis is on presenting the possibility of catalytic behaviour carried out in the almost complete absence of environmental turbulence, thus, the units' morphology with respect to each reaction phase could be discussed. This aspect of the system, that it develops rather statically, at the same time, indicates that the mechanism shows a potential for smaller scales at which the influence of mass is more negligible. Incorporation of stochasticity through externally added kinetic turbulence or water agitation could nevertheless be feasible. By sufficiently shortening R2 in figure 1*c*, but still conserving the condition that R1 < R2, such environmental perturbation may still be able to invoke a sliding motion of M_2, thus realizing conformation change of $\mathcal{S}$.

Regulating the agitation level and investigating the influence of catalytic enhancement would be of interest in future research.

6. Conclusion

With a special focus on the role of morphology, this study approaches the realization of a fully functional centimetre-sized, mechanical model of catalysis. We report on the construction and operation of the model, which contains both *enzymes* and *inhibitors*. To illustrate the analogous underlying processes of enzymatic behaviour, we first formulate the intermagnetic interactions attainable with permanent magnets. Then, we introduce physical units that instantiate the interaction and validate the desired behaviour where an *enzyme* triggers a kinematic reconfiguration of the target units, funnelling down the magnetic potential barrier (activation potential), whereas an *inhibitor* inhibits a reconfiguration by creating a barrier. As this phenomenon was attained at the pure physics level by combining morphology and magnetism, this study provides a platform at the intersection of classical mechanics (unit design), physics (magnetism) and chemistry (enzyme reaction). The obtained model extends the conventional definition of catalysis to systems of alternative scales, realizing 'mechanical' reactions with hands-on artefacts, which can expand the concept of manufacturing.

Funding statement. This work was partially supported by a Swiss National Science Foundation Fellowship number PA00P2_142208.

Endnote

[1]The CAD data of all the designed units can be downloaded as electronic material in STL file format at http://www.shuhei.net/.

References

1. Berg JM, Tymoczko JL, Stryer L. 2002 *Biochemistry*, 5th edn. New York, NY: W H Freeman.
2. Alberts B, Johnson A, Lewis J, Raff M, Roberts K, Walter P. 2002 *Molecular biology of the cell*, 4th edn. New York, NY: Garland Science.
3. Whitesides GM, Grzybowski B. 2002 Self-assembly at all scales. *Science* **295**, 2418–2421. (doi:10.1126/science.1070821)
4. Boncheva M, Whitesides GM. 2005 Making things by self-assembly. *MRS Bull.* **30**, 736–742. (doi:10.1557/mrs2005.208)
5. Cohn MB, Kim CJ. 1991 Self-assembling electrical networks: an application of micromachining technology. In *Proc. Int. Conf. Solid-State Sensor Actuat.* (*Transducers*), *San Francisco, CA, USA, June 24–27 1991*. Piscataway, NJ: IEEE.
6. Pierce CS. 1878 Floating magnets. *Nature* **18**, 381. (doi:10.1038/018381a0)
7. Shetye SB, Eskinazi I, Arnold DP. 2008 Self-assembly of millimeter-scale components using integrated micromagnets. *IEEE Trans. Magn.* **44**, 4293–4296. (doi:10.1109/TMAG.2008.2001344)
8. Ramadan Q, Uk YS, Vaidyanathan K. 2007 Large scale microcomponents assembly using an external magnetic array. *Appl. Phys. Lett.* **90**, 172502. (doi:10.1063/1.2731708)
9. Miyashita S, Nagy Z, Nelson BJ, Pfeifer R. 2009 The influence of shape on parallel self-assembly. *Entropy* **11**, 643–666. (doi:10.3390/e11040643)
10. Miyashita S, Diller E, Sitti M. 2013 Two dimensional micro-scale magnetic reconfiguration based on intra-module interactions. *Int. J. Robot. Res.* **32**, 591–615. (doi:10.1177/0278364913479837)
11. Böhringer KF, Goldberg K, Cohn M, Howe R, Pisano A. 1998 Parallel microassembly with electrostatic force fields. In *IEEE Int. Conf. Robot. Autom.* (*ICRA*), *Leuven, Belgium, May 16–20 1998*. Piscataway, NJ: IEEE.
12. Grzybowski BA, Winkleman A, Wiles JA, Brumer Y, Whitesides GM. 2003 Electrostatic self-assembly of macroscopic crystals using contact electrification. *Nat. Mater.* **2**, 241–245. (doi:10.1038/nmat860)
13. Hosokawa K, Shimoyama I, Miura H. 1996 Two-dimensional micro-self-assembly using the surface tension of water. *Sensor Actuat. A* **57**, 117–125. (doi:10.1016/S0924-4247(97)80102-1)
14. Bowden N, Terfort A, Carbeck J, Whitesides GM. 1997 Self-assembly of mesoscale objects into ordered two-dimensional arrays. *Science* **276**, 233–235. (doi:10.1126/science.276.5310.233)
15. Rothemund PWK. 2000 Using lateral capillary forces to compute by self-assembly. *Proc. Natl Acad. Sci. USA* **97**, 984–989. (doi:10.1073/pnas.97.3.984)
16. Wolfe DB, Snead A, Mao C, Bowden NB, Whitesides GM. 2003 Mesoscale self-assembly: capillary interactions when positive and negative menisci have similar amplitudes. *Langmuir* **19**, 2206–2214. (doi:10.1021/la0264973)
17. Park S, Lim JH, Chung SW, Mirkin CA. 2004 Self-assembly of mesoscopic metal-polymer amphiphiles. *Science* **303**, 348–351. (doi:10.1126/science.1093276)
18. Randhawa JS, Kanu LN, Singh G, Gracias DH. 2010 Importance of surface patterns for defect mitigation in three-dimensional self-assembly. *Langmuir* **26**, 12 534–12 539. (doi:10.1021/la101188z)
19. Grzybowski BA, Stone HA, Whitesides GM. 2000 Dynamic self-assembly of magnetized, millimetre-sized objects rotating at a liquid–air interface. *Nature* **405**, 1033–1036. (doi:10.1038/35016528)
20. Gracias DH, Tien J, Breen TL, Hsu C, Whitesides GM. 2000 Forming electrical networks in three dimensions by self-assembly. *Science* **289**, 1170–1172. (doi:10.1126/science.289.5482.1170)
21. Boncheva M, Gracias DH, Jacobs HO, Whitesides GM. 2002 Biomimetic self-assembly of a functional asymmetrical electronic device. *Proc. Natl Acad. Sci. USA* **99**, 4937–4940. (doi:10.1073/pnas.032667599)
22. Jacobs HO, Tao AR, Schwartz A, Gracias DH, Whitesides GM. 2002 Fabrication of a cylindrical display by patterned assembly. *Science* **296**, 323–325. (doi:10.1126/science.1069153)
23. Boncheva M, Ferrigno R, Bruzewicz DA, Whitesides GM. 2003 Plasticity in self-assembly: templating generates functionally different circuits from a single precursor. *Angew. Chem. Int. Ed.* **42**, 3368–3371. (doi:10.1002/anie.200351533)
24. Stambaugh J, Lathrop DP, Ott E, Losert W. 2003 Pattern formation in a monolayer of magnetic spheres. *Phys. Rev. E* **68**, 026207. (doi:10.1103/PhysRevE.68.026207)
25. Mao C, Thalladi VR, Wolfe DB, Whitesides S, Whitesides GM. 2002 Dissections: self-assembled aggregates that spontaneously reconfigure their structures when their environment changes. *J. Am. Chem. Soc.* **124**, 14 508–14 509. (doi:10.1021/ja021043d)
26. Dejeu J, Rougeot P, Gauthier M, Boireau W. 2009 Robotic submerged microhandling controlled by pH switching. In *IEEE/RSJ Int. Conf. Intell. Robots Sys.* (*IROS*), *St. Louis, MO, USA, October 11–15 2009*. Piscataway, NJ: IEEE.
27. Shaw RS, Packard N, Schröter M, Swinney HL. 2007 Geometry-induced asymmetric diffusion. *Proc. Natl Acad. Sci. USA* **104**, 9580–9584. (doi:10.1073/pnas.0703280104)
28. Penrose LS. 1959 Self-reproducing machines. *Sci. Am.* **200**, 105–114. (doi:10.1038/scientificamerican0659-105)
29. Breivik J. 2001 Self-organization of template-replicating polymers and the spontaneous rise of genetic information. *Entropy* **3**, 273–279. (doi:10.3390/e3040273)
30. Matsumoto M, Hashimoto S. 2009 Passive self-replication of millimeter-scale parts. *Proc. IEEE Trans. Autom. Sci. Eng.* **6** 385–391. (doi:10.1109/TASE.2008.2006625)
31. Virgo N, Fernando C, Bigge B, Husbands P. 2012 Evolvable physical self-replicators. *Artif. Life* **18**, 129–142. (doi:10.1162/artl_a_00056)
32. Hosokawa K, Shimoyama I, Miura H. 1994 Dynamics of self-assembling systems: analogy with chemical kinetics. *Artif. Life* **1**, 413–427. (doi:10.1162/artl.1994.1.413)
33. Tsutsumi D, Murata S. 2007 Multistate part for mesoscale self-assembly. In *SICE Annual Conf. Kagawa, Japan, September 17–20 2007*. Piscataway, NJ: IEEE.